Direct observation of atomic configuration of a highly oriented MoS_2 film/α-Al_2O_3 (0001) using atomic resolution electron microscopy

Emi Kano,[1] Jun Nara,[2] Koki Takenaka,[3] Toshiki Yasuno,[3] Keisuke Atsumi,[4] Shuhong Li,[4] Tomonori Nishimura,[4] Kaito Kanahashi,[4] Jun Uzuhashi,[5] Kosuke Nagashio,[4] Yoshiki Sakuma,[6] Nobuyuki Ikarashi[1]

[1] Institute of Materials and Systems for Sustainability, Nagoya University, Nagoya, Aichi 464-8601, Japan
[2] Research Center for Materials Nanoarchitectonics, National Institute for Materials Science, 1-1 Namiki, Tsukuba 305-0044, Japan
[3] Graduate School of Engineering, Nagoya University, Nagoya, Aichi 464-8603, Japan
[4] Department of Materials Engineering, The University of Tokyo, 7-3-1 Hongo, Bunkyo-ku, Tokyo 113-8656, Japan
[5] Electron Microscopy Unit, National Institute for Materials Science, 1-2-1 Sengen, Tsukuba, Ibaraki 305-0047, Japan
[6] Research Center for Electronic and Optical Materials, National Institute for Materials Science, 1-1 Namiki, Tsukuba 305-0044, Japan

Corresponding author: Emi Kano
Email: kano@imass.nagoya-u.ac.jp

<Abstract>

We deposited a highly oriented MoS_2 film on a 2-inch α-Al_2O_3 (0001) wafer by metal-organic chemical vapor deposition and determined the atomic configuration of the MoS_2/α-Al_2O_3 (0001) stacking structure by performing atomic resolution electron microscopy observations along two orthogonal zone axis directions, i.e., the $\langle 11\bar{2}0 \rangle$ and $\langle 1\bar{1}00 \rangle$ directions of α-Al_2O_3. The results show that, first, the in-plane positions of Mo atoms coincide with those of the underlying Al and O atoms, and the $[11\bar{2}0]$ direction of monolayer 2H-MoS_2 matches that of the α-Al_2O_3 substrate. Second, the α-Al_2O_3 surface was a reconstructed Al-I structure. Moreover, we performed the first-principles calculations using the observed in-plane atomic positions of the MoS_2/α-Al_2O_3 structure as a starting configuration and found that the MoS_2 –Al_2O_3 distance is larger than the theoretical van der Waals distance. Because no ordered structures were observed between the MoS_2 film and the Al_2O_3 substrate, the experimental and theoretical results strongly suggest that an amorphous interface layer exists between them. Such an amorphous interface layer is likely to weaken the MoS_2–Al_2O_3 interaction that determines the stability of the MoS_2/α-Al_2O_3 (0001) structure. We thus argue that controlling the interface layer is critical in fabricating highly oriented MoS_2 films and is vital for improving the performance of field-effect transistors with MoS_2 channels.

Si metal-semiconductor-oxide field-effect transistors (MOS-FETs) have been scaled down to improve device performance at reduced power and cost. Along the geometrical scaling path, the MOS-FET structure has changed from bulk-planar to gate-all-around, which could eliminate short-channel effects at reduced gate lengths.[1] [2] On the other hand, the mobility of charge carriers in conventional semiconductors, such as Si and SiGe, decreases as the channel body thickness is made smaller.[3] Here, transition metal dichalcogenides (TMDs) show great potential as channel materials for deeply scaled MOS-FETs because they can be used to make an atomically thin body and are theoretically predicted to have high carrier mobility.[3] [4] [5] [6] [7] [8] [9]

For fabricating large-scale integrated circuits with TMD channels, wafer-scale TMD films with improved transport properties are necessary. Previous studies have indicated that defects in TMD films, such as grain boundaries have a major impact on transport properties.[10] [11] We have grown monolayer MoS_2 film on α-Al_2O_3 by metal-organic chemical vapor deposition (MOCVD) and have shown that highly oriented or single crystalline MoS_2 films exhibit phonon-limited mobility, while polycrystalline MoS_2 films exhibit thermally activated mobility.[12] These indicate that control of the crystalline orientation of TMD films is critical to controlling their transport properties.

The orientation of TMD films is substantially influenced by the crystallographic structure of the substrate,[13] [14] [15] and various models have been proposed for the TMD–substrate interaction that determines the orientation of the films. However, the underlying mechanism is still under debate. For example, some models assume an interaction through an interface layer, such as a crystalline thin film or a layer of regularly arranged atoms or molecules,[16] [17] [18] [19] [20] [21] while others assume no interface layer and instead postulate a direct van der Waals interaction.[14] [22] [23] In addition, some studies[14] [16] [22] [23] on TMDs grown on α-Al_2O_3 (0001) substrates have assumed an Al-I surface structure[24], while others[18] [19] [21] have assumed an Al-II surface structure. α-Al_2O_3 (0001) wafers have often been used because of their chemical stability under TMD growth conditions and the availability of large-diameter wafers. This variety of proposed TMD/substrate structural models is mainly due to the lack of experimental results showing the atomic configuration of the TMD/substrate stacking structure. That is, the structural features that determine the stability of the structure, such as the positions of atoms of a TMD film along the TMD/substrate interface (or the in-plane atomic positions of a TMD film on a substrate), the surface structure of the substrate, and the structure of the interface layer, if it exists, have yet to be clarified.

Here, we report a definitive structural analysis on the atomic configuration of the MOCVD-grown MoS_2/α-$Al_2O_3(0001)$ stacking structure. We prepared a highly oriented, almost single-crystalline, monolayer MoS_2 film with reduced electrically active defects and analyzed it using atomic resolution transmission electron microscopy (TEM) and first-principles calculations. The experimental results clarified the in-plane atomic positions of the MoS_2 film/α-Al_2O_3 structure, the surface structure of α-Al_2O_3 substrate, and the MoS_2–α-Al_2O_3 distance. Moreover, the experimental and theoretical analyses strongly suggest the existence of an amorphous interface layer. We thus argue that controlling the interface layer is critical for fabricating highly oriented TMD films and improving the performance of field-effect transistors with MoS_2 channels.

A MoS_2 film was grown by MOCVD, where MoO_2Cl_2 and H_2S were used as precursors, and N_2 was used as carrier gas. We used a 2-inch α-Al_2O_3 (0001) wafer as a substrate and annealed it at 1150°C in air for 1 hour prior to the growth of MoS_2. After annealing in air at temperatures above 1000 °C, Al_2O_3 (0001) surfaces reportedly exhibit a terrace-step morphology with atomically flat terraces,[17 25 26] and the surface is crystalline.[25] Thus, no amorphous layer was likely to exist on the substrate surface before the MoS_2 growth, although we did not examine the atomic structure of the substrate surface. The substrate temperature was 950°C during the growth. Figure 1 shows a plan-view TEM image and a transmission electron diffraction (TED) pattern of the MoS_2 film transferred onto a holey carbon TEM grid (Quantifoil 1.2/1.3), and the holes are empty. The TED pattern (inset) shows a single set of six $1\bar{1}00$ spots of MoS_2 and no spots due to rotational domains, indicating that the film was almost single crystalline and that the portion of the rotational domains were very small. The micrograph shows a $1\bar{1}00$ dark-field (DF) image taken from a specimen area where rotational domains were observed. The dark and light gray regions (arrowed) are rotational and 180° rotational domains, respectively, and the white and gray triangles are double-layer regions. Thus, Fig. 1 shows that most of the MoS_2 film was a single crystal with a monolayer thickness, although a small part of the film was rotational or double-layer domains with nanometer-scale lateral dimensions. The electrically active defects in the MoS_2 film were well reduced, and the film exhibited phonon-limited mobility.[12]

Atomic resolution observations were performed using high-angle annular dark-field scanning TEM (HAADF-STEM). The acceleration voltage was 200 kV, and the spherical aberration coefficient was less than 1 μm. The inner and outer angles of the

annular dark-field detector were 50 and 150 mrad, respectively. Cross-sectional TEM specimens were prepared by mechanical thinning and Ar ion milling.

We performed first-principles calculations based on density-functional theory (DFT) [27] and pseudo-potential schemes using the PHASE/0 code[28]. The generalized gradient approximation of Perdew, Burke, and Ernzerhof was used as the exchange-correlation energy functional.[29] As for the van der Waals interactions, the DFT-D2 method was applied.[30] We used a slab model consisting of monolayer MoS_2 on an α-Al_2O_3 (0001). The in-plane periodicity of the 3×3 MoS_2 and 2×2 α-Al_2O_3 unit cells were fixed. The Al_2O_3 slab contains twelve Al layers, and the top and bottom of the slab were terminated with a single Al layer in accordance with the present experimental results. Details of the model structure are described in the following. The cut-off energies for the wavefunctions and charge density were 56 Ry and 506 Ry, respectively. The number of *k* points sampled in the Brillouin zone was more than 2×2 per surface unit cell of α-Al_2O_3 (0001). All the models were optimized to meet the force criteria of 0.01 eV/Å.

HAADF-STEM images of the MoS_2/α-Al_2O_3 (0001) structure viewed in the $\langle 1\bar{1}00 \rangle$ and $\langle 11\bar{2}0 \rangle$ directions of α-Al_2O_3 are shown in Fig. 2(a) and 2(b). Bright dots in the images are at the positions of Mo, S, Al, and O atoms. O atoms of the α-Al_2O_3 substrate are only weaky seen in Fig. 2(b), because the number of atoms at each O atom position is only half of that of the Al atoms in the incident beam direction. In Fig. 2(a), Mo atoms are located atop the Al $(11\bar{2}0)$ planes indicated by the vertical dotted lines. In Fig. 2(b), they are atop the Al $(1\bar{1}00)$ planes indicated by the vertical dashed lines. In addition, in Fig. 2(b), the lateral (in the $\langle 1\bar{1}00 \rangle$ direction) distance between a Mo and neighboring S atoms is smaller on the left-hand side of the Mo atom than on the right-hand side, directly indicating that the $[11\bar{2}0]$ direction of monolayer 2H-MoS_2 matches that of the α-Al_2O_3 substrate. Thus, the in-plane positions of the Mo and S atoms of the MoS_2 film on the α-Al_2O_3 substrate are as depicted in Fig. 2(c), which schematically shows the MoS_2/α-Al_2O_3 structure viewed in the $\langle 0001 \rangle$ direction. The dashed and dotted lines in the figure correspond to the positions of the Al planes indicated by the dotted or dashed lines in Fig. 2(a) and 2(b). Thus, Fig. 2(c) shows that the in-plane positions of Mo atoms coincide with those of the underlying Al and O atoms.

In the lateral direction in Fig. 2(a) and (b), the three-fold length of the period of the MoS_2 lattice image coincides with the two-fold length of the period of the Al_2O_3 lattice image. This implies that the in-plane atomic spacing of the MoS_2 film is +0.2% of its

literature value in both the $\langle 1\bar{1}00\rangle$ and $\langle 11\bar{2}0\rangle$ directions, provided that the lattice constant of Al_2O_3 remains unchanged.[31] [32] However, further experiments are needed to clarify the strain of the MoS_2 film quantitatively.

In addition, the HAADF-STEM images of the α-Al_2O_3 surface indicate that the surface is Al-I terminated. In Fig. 2(b), bright dots are at Al atom positions in the Al_2O_3 substrate. The topmost Al layer comprises a single Al atomic layer, denoted as T, while closely spaced pairs of Al atomic layers, denoted as D_1, D_2, and D_3, are in the bulk. This indicates that the substrate surface is Al-I terminated, differing from the Al-II and O-I terminated structures[24], as well as from the O-terminated or OH-terminated structures proposed as the surface structures under CVD growth conditions[23]. Moreover, no periodic structures can be seen between the MoS_2 film and the Al_2O_3 surface in the HAADF-STEM images in Figs. 2. This strongly suggests that the MoS_2 film and the Al_2O_3 substrate are separated by a vacuum layer or an amorphous layer, not by a layer with the ordered structures that have been suggested in previous studies.[16] [17] [18] [19] [20] [21]

To quantitatively determine the atomic layer spacing in the MoS_2/α-Al_2O_3 structure, we measured the image intensities in the HAADF-STEM images. Figure 3(a) shows a magnified image of the MoS_2/α-Al_2O_3 structure, and Fig. 3(b) shows the image intensity profile in the depth direction ([0001] direction), averaged over 2 nm parallel to the interface. The peak denoted as Mo in the diagram represents the position of the Mo layer. The peak denoted as T is at the positions of the surface Al layer and those denoted as D_n (n = 1 to 7) are at the closely spaced Al atomic layer pairs. Gaussian fits to these peaks (Fig. 3(c)) were used to determine the peak positions, from which the layer spacings were extracted (Fig. 3(d)). The spacing between neighboring D_n peaks is 0.22 nm on average and is nearly constant, corresponding to the spacing between Al-layer pairs of α-Al_2O_3.[31] Minor fluctuations are attributed to experimental noise. The Mo–T spacing is 0.86 ± 0.06 nm on average across five measurements in distinct observation areas. In addition, the T–D_1 spacing is 0.16 nm, i.e., 72% of the spacing between the D_n peaks. These spacings are listed in Table I together with those of the theoretical models described below.

Table I Experimental and theoretical (model A and B) atomic layer spacings in nanometer. Experimental values show average and standard deviation of layer spacings measured on HAADF-STEM images.

Layer spacing	Experimental	Model	
		A	B
Mo–T	0.86 ± 0.06	0.43	–
T–D_1	0.16 ± 0.02	0.11	0.11
D_n–D_{n+1}	0.22 ± 0.01	0.22	0.22

We further explored the atomic configurations of the MoS_2/α-Al_2O_3 structure by performing first-principles calculations using an atomic model with the experimentally determined in-plane positions of the MoS_2/α-Al_2O_3 structure as a starting configuration (model A). No interface layer was assumed in the calculation. We also performed structural optimization of a model without a MoS_2 layer, i.e., the clean Al-I surface model (model B). The atomic configurations of the relaxed structures of the models are depicted in Fig. 4 and the atomic layer spacings are listed in Table I. We used the positions of the atoms of each atomic layer (Mo, ~~S~~T, and D_n layers) averaged in the ⟨0001⟩ direction as the atomic layer positions, from which their spacings were extracted.

Table I shows that the observed Mo–T spacing is larger than that of model A. This indicates that the space between the MoS_2 film and the substrate in the present sample is not a vacuum, but an interface layer is likely to exist between them. Thus, the observed Mo–T spacing and HAADF-STEM image in Fig. 2 indicate that an amorphous interface layer exists between the MoS_2 film and the substrate. In addition, the observed T–D_1 spacing differs from that of model A and also differs from that of the truncated (pristine) Al-I surface (0.19 nm). This indicates that the surface Al-I layer is reconstructed through an interaction between the surface Al-I layer and the interface layer on it. Therefore, the Mo–T and T–D_1 layer spacings in Table I strongly suggest that an amorphous interface layer exists between the MoS_2 film and substrate and it affects the Al-I surface structure of the substrate.

The present analysis has clarified the atomic configuration of the highly oriented MoS_2/α-Al_2O_3 structure. The epitaxial relationship on the atomic scale shows that the interaction between the MoS_2 film and the substrate plays a pivotal role in determining

the MoS_2 orientation. On the other hand, the amorphous interface layer found between the film and substrate is likely to weaken the interaction, and thus, when an interface layer that further weakens the interaction forms, the portion of the rotational domains in the MoS_2 film would increase. Previous studies have shown that the orientation of MoS_2 changes depending on substrate surface conditions and the MoS_2 growth conditions[16-23]. These suggest that the properties of the interface layers can be controlled through these conditions. Therefore, controlling the interface layer during MoS_2 growth is critical for fabricating highly oriented MoS_2 films and for improving their transfer characteristics.

In summary, a highly oriented monolayer-MoS_2/α-Al_2O_3 grown by MOCVD has been analyzed by atomic resolution HAADF-STEM direct observations combined with first-principles calculations. The observations have directly clarified the epitaxial relation between MoS_2 and α-Al_2O_3: the in-plane positions of the Mo atoms coincide with those of the underlying Al and O atoms, and the [11-20] direction of the monolayer 2H-MoS_2 matches that of the α-Al_2O_3 substrate. In addition, the observed α-Al_2O_3 surface was a reconstructed Al-I surface. Moreover, the results showing that the observed MoS_2–α-Al_2O_3 distance was larger than the theoretical van der Waals distance and that no ordered structures were observed between the MoS_2 film and α-Al_2O_3 substrate strongly suggest that an amorphous interface layer existed between the MoS_2 film and α-Al_2O_3 substrate. Such an interface layer is likely to weaken the interaction between the MoS_2 film and α-Al_2O_3 substrate. We thus argue that control of the interface layer is critical to growing a unidirectional MoS_2 film on α-Al_2O_3 substrate.

Supplementary material

The supplementary material describes the simulated STEM image of model A and the energy dispersive X-ray spectroscopy line profile across the interface layer between MoS_2 and Al_2O_3 for the sample deposited under growth conditions nearly equivalent to those of the sample described in the main text.

Acknowledgements

This work was partly supported by JSPS KAKENHI (Grant Numbers: JP21H05237, JP21H05232, JP22H04957), the JST-Mirai Program (Grant Number: JPMJMI22708192), and JST CREST (Grant Number: JPMJCR24A3). Calculations were performed on the Numerical Materials

Simulator of NIMS and ES of JAMSTEC. A part of this work was supported by the Electron Microscopy Unit, NIMS.

Data availability statement

The data that supports the findings of this study are available within the article and its supplementary material.

References

[1] N. Loubet, T. Hook, P. Montanini, C.-W. Yeung, S. Kanakasabapathy, M. Guillom, T. Yamashita, J. Zhang, X. Miao, J. Wang, A. Young, R. Chao, M. Kang, Z. Liu, S. Fan, B. Hamieh, S. Sieg, Y. Mignot, W. Xu, S.-C. Seo, J. Yoo, S. Mochizuki, M. Sankarapandian, O. Kwon, A. Carr, A. Greene, Y. Park, J. Frougier, R. Galatage, R. Bao, J. Shearer, R. Conti, H. Song, D. Lee, D. Kong, Y. Xu, A. Arceo, Z. Bi, P. Xu, R. Muthinti, J. Li, R. Wong, D. Brown, P. Oldiges, R. Robison, J. Arnold, N. Felix, S. Skordas, J. Gaudiello, T. Standaert, H. Jagannathan, D. Corliss, M.-H. Na, A. Knorr, T. Wu, D. Gupta, S. Lian, R. Divakaruni, T. Gow, C. Labelle, S. Lee, V. Paruchuri, H. Bu, and M. Khare, "Stacked nanosheet gate-all-around transistor to enable scaling beyond FinFET," in *2017 Symp. VLSI Technol.*, (IEEE, 2017), pp. T230–T231.

[2] IRDS, *International Roadmap for Devices and Systems* (IEEE, 2024).

[3] D. Akinwande, C. Huyghebaert, C.H. Wang, M.I. Serna, S. Goossens, L.J. Li, H.S.P. Wong, and F.H.L. Koppens, "Graphene and two-dimensional materials for silicon technology," Nature **573**(7775), 507–518 (2019).

[4] K. Kaasbjerg, K.S. Thygesen, and K.W. Jacobsen, "Phonon-limited mobility in n-type single-layer MoS 2 from first principles," Phys. Rev. B - Condens. Matter Mater. Phys. **85**(11), 1–16 (2012).

[5] M.W. Iqbal, M.Z. Iqbal, M.F. Khan, M.A. Shehzad, Y. Seo, J.H. Park, C. Hwang, and J. Eom, "High-mobility and air-stable single-layer WS2 field-effect transistors sandwiched between chemical vapor deposition-grown hexagonal BN films," Sci. Rep. **5**(June), 1–9 (2015).

[6] W. Cao, H. Bu, M. Vinet, M. Cao, S. Takagi, S. Hwang, T. Ghani, and K. Banerjee, "The future transistors," Nature **620**(7974), 501–515 (2023).

[7] K.P. O'Brien, C.H. Naylor, C. Dorow, K. Maxey, A.V. Penumatcha, A. Vyatskikh, T. Zhong, A. Kitamura, S. Lee, C. Rogan, W. Mortelmans, M.S. Kavrik, R. Steinhardt, P. Buragohain, S. Dutta, T. Tronic, S. Clendenning, P. Fischer, E.S. Putna, M. Radosavljevic, M. Metz, and U. Avci, "Process integration and future outlook of 2D transistors," Nat. Commun. **14**(1), 6400 (2023).

[8] C.J. Dorow, T. Schram, Q. Smets, K.P. O'Brien, K. Maxey, C.-C. Lin, L. Panarella, B. Kaczer, N. Arefin, A. Roy, R. Jordan, A. Oni, A. Penumatcha, C.H. Naylor, M. Kavrik, D. Cott, B. Graven, V. Afanasiev, P. Morin, I. Asselberghs, C.J. Lockhart de La Rosa, G. Sankar Kar, M. Metz, and U. Avci, "Exploring manufacturability of novel 2D channel materials: 300 mm wafer-scale 2D NMOS & PMOS using MoS 2 , WS 2 , & WSe 2," in *2023 Int. Electron Devices Meet.*, (IEEE, 2023), pp. 1–4.

[9] P. Wu, T. Zhang, J. Zhu, T. Palacios, and J. Kong, "2D materials for logic device scaling," Nat. Mater. **23**(1), 23–25 (2024).

[10] T.H. Ly, D.J. Perello, J. Zhao, Q. Deng, H. Kim, G.H. Han, S.H. Chae, H.Y. Jeong, and Y.H. Lee, "Misorientation-angle-dependent electrical transport across molybdenum disulfide grain boundaries," Nat. Commun. **7**, 1–7 (2016).

[11] S. Somay, and K. Balasubramanian, “Defect structure-electronic property correlations in transition metal dichalcogenide grain boundaries,” Phys. Chem. Chem. Phys. **26**(29), 19787–19794 (2024).
[12] Y. Sakuma, K. Atsumi, T. Hiroto, J. Nara, A. Ohtake, Y. Ono, T. Matsumoto, E. Kano, T. Yasuno, X. Yang, N. Ikarashi, A. Suzuki, M. Ikezawa, S. Li, T. Nishimura, K. Kanahashi, and K. Nagashio, “Self-aligned and self-limiting van der Waals epitaxy of monolayer MoS 2 to annihilate grain boundaries for scalable 2D electronics,” Nat. Commun., 1–24 (n.d.).
[13] J. Dong, L. Zhang, X. Dai, and F. Ding, “The epitaxy of 2D materials growth,” Nat. Commun. **11**(1), 5862 (2020).
[14] P. Zheng, W. Wei, Z. Liang, B. Qin, J. Tian, J. Wang, R. Qiao, Y. Ren, J. Chen, C. Huang, X. Zhou, G. Zhang, Z. Tang, D. Yu, F. Ding, K. Liu, and X. Xu, “Universal epitaxy of non-centrosymmetric two-dimensional single-crystal metal dichalcogenides,” Nat. Commun. **14**(1), 592 (2023).
[15] C. Liu, T. Liu, Z. Zhang, Z. Sun, G. Zhang, E. Wang, and K. Liu, “Understanding epitaxial growth of two-dimensional materials and their homostructures,” Nat. Nanotechnol. **19**(7), 907–918 (2024).
[16] Y. Xiang, X. Sun, L. Valdman, F. Zhang, T.H. Choudhury, M. Chubarov, J.A. Robinson, J.M. Redwing, M. Terrones, Y. Ma, L. Gao, M.A. Washington, T.-M. Lu, and G.-C. Wang, “Monolayer MoS 2 on sapphire: an azimuthal reflection high-energy electron diffraction perspective,” 2D Mater. **8**(2), 025003 (2021).
[17] L. Liu, T. Li, L. Ma, W. Li, S. Gao, W. Sun, R. Dong, X. Zou, D. Fan, L. Shao, C. Gu, N. Dai, Z. Yu, X. Chen, X. Tu, Y. Nie, P. Wang, J. Wang, Y. Shi, and X. Wang, “Uniform nucleation and epitaxy of bilayer molybdenum disulfide on sapphire,” Nature **605**(7908), 69–75 (2022).
[18] H. Zhu, N. Nayir, T.H. Choudhury, A. Bansal, B. Huet, K. Zhang, A.A. Puretzky, S. Bachu, K. York, T. V. Mc Knight, N. Trainor, A. Oberoi, K. Wang, S. Das, R.A. Makin, S.M. Durbin, S. Huang, N. Alem, V.H. Crespi, A.C.T. van Duin, and J.M. Redwing, “Step engineering for nucleation and domain orientation control in WSe2 epitaxy on c-plane sapphire,” Nat. Nanotechnol. **18**(11), 1295–1302 (2023).
[19] J.H. Fu, J. Min, C.K. Chang, C.C. Tseng, Q. Wang, H. Sugisaki, C. Li, Y.M. Chang, I. Alnami, W.R. Syong, C. Lin, F. Fang, L. Zhao, T.H. Lo, C.S. Lai, W.S. Chiu, Z.S. Jian, W.H. Chang, Y.J. Lu, K. Shih, L.J. Li, Y. Wan, Y. Shi, and V. Tung, “Oriented lateral growth of two-dimensional materials on c-plane sapphire,” Nat. Nanotechnol. **18**(11), 1289–1294 (2023).
[20] A. Aljarb, J. Min, M. Hakami, J.H. Fu, R. Albaridy, Y. Wan, S. Lopatin, D. Kaltsas, D. Naphade, E. Yengel, M.N. Hedhili, R. Sait, A.H. Emwas, A. Kutbee, M. Alsabban, K.W. Huang, K. Shih, L. Tsetseris, T.D. Anthopoulos, V. Tung, and L.J. Li, “Interfacial Reconstructed Layer Controls the Orientation of Monolayer Transition-Metal Dichalcogenides,” ACS Nano **17**(11), 10010–10018 (2023).
[21] L. Li, Q. Wang, F. Wu, Q. Xu, J. Tian, Z. Huang, Q. Wang, X. Zhao, Q. Zhang, Q. Fan, X. Li, Y. Peng, Y. Zhang, K. Ji, A. Zhi, H. Sun, M. Zhu, J. Zhu, N. Lu, Y. Lu, S. Wang, X. Bai, Y. Xu, W. Yang, N. Li, D. Shi, L. Xian, K. Liu, L. Du, and G. Zhang, “Epitaxy of wafer-scale single-crystal MoS2 monolayer via buffer layer control,” Nat. Commun. **15**(1), 1825 (2024).

[22] T. Li, W. Guo, L. Ma, W. Li, Z. Yu, Z. Han, S. Gao, L. Liu, D. Fan, Z. Wang, Y. Yang, W. Lin, Z. Luo, X. Chen, N. Dai, X. Tu, D. Pan, Y. Yao, P. Wang, Y. Nie, J. Wang, Y. Shi, and X. Wang, "Epitaxial growth of wafer-scale molybdenum disulfide semiconductor single crystals on sapphire," Nat. Nanotechnol. **16**(11), 1201–1207 (2021).

[23] Y. Park, C. Ahn, J.G. Ahn, J.H. Kim, J. Jung, J. Oh, S. Ryu, S. Kim, S.C. Kim, T. Kim, and H. Lim, "Critical Role of Surface Termination of Sapphire Substrates in Crystallographic Epitaxial Growth of MoS2 Using Inorganic Molecular Precursors," ACS Nano **17**(2), 1196–1205 (2023).

[24] T. Kurita, K. Uchida, and A. Oshiyama, "Atomic and electronic structures of α -Al2 O3 surfaces," Phys. Rev. B - Condens. Matter Mater. Phys. **82**(15), 1–14 (2010).

[25] M. Yoshimoto, T. Maeda, T. Ohnishi, H. Koinuma, O. Ishiyama, M. Shinohara, M. Kubo, R. Miura, and A. Miyamoto, "Atomic-scale formation of ultrasmooth surfaces on sapphire substrates for high-quality thin-film fabrication," Appl. Phys. Lett. **67**(18), 2615–2617 (1995).

[26] F. Cuccureddu, S. Murphy, I. V. Shvets, M. Porcu, H.W. Zandbergen, N.S. Sidorov, and S.I. Bozhko, "Surface morphology of c-plane sapphire (α-alumina) produced by high temperature anneal," Surf. Sci. **604**(15–16), 1294–1299 (2010).

[27] W. Kohn, and L.J. Sham, "Self-Consistent Equations Including Exchange and Correlation Effects," Phys. Rev. **140**(4A), A1133–A1138 (1965).

[28] T. Yamasaki, A. Kuroda, T. Kato, J. Nara, J. Koga, T. Uda, K. Minami, and T. Ohno, "Multi-axis decomposition of density functional program for strong scaling up to 82,944 nodes on the K computer: Compactly folded 3D-FFT communicators in the 6D torus network," Comput. Phys. Commun. **244**, 264–276 (2019).

[29] J.P. Perdew, K. Burke, and M. Ernzerhof, "Generalized gradient approximation made simple," Phys. Rev. Lett. **77**(18), 3865–3868 (1996).

[30] S. Grimme, "Semiempirical GGA-type density functional constructed with a long-range dispersion correction," J. Comput. Chem. **27**(15), 1787–1799 (2006).

[31] E.N. Maslen, V.A. Streltsov, N.R. Streltsova, N. Ishizawa, and Y. Satow, "Synchrotron X-ray study of the electron density in α-Al2O3," Acta Crystallogr. Sect. B **49**(6), 973–980 (1993).

[32] R.W.G. Wyckoff, *Crystal Structures*, 2nd ed. (Interscience Publishers, New York, 1963).

<Figure>

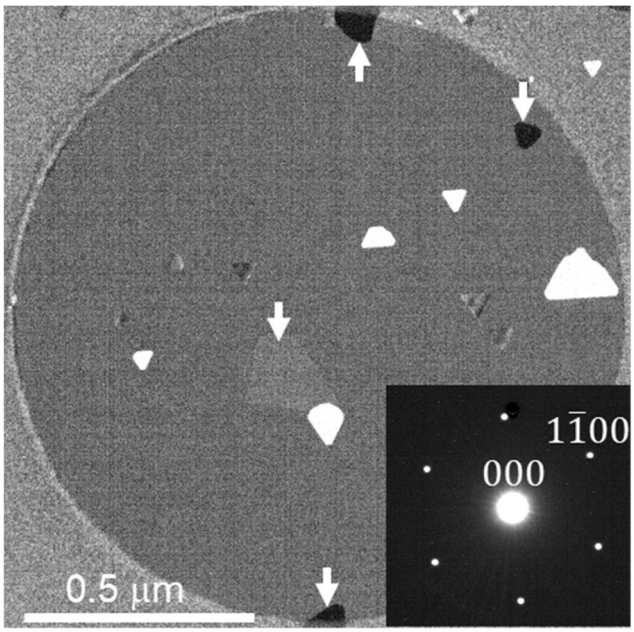

Fig. 1 Example of a plan-view $1\bar{1}00$ DF image of rotational domains of MoS_2 film and a TED pattern (inset) taken from a large specimen area. The TED pattern shows a single set of six $1\bar{1}00$ spots, indicating that portion of the rotational domains are very small. Dark and light-gray regions in the DF image (arrows) are rotational and 180° rotational domains, respectively. White and gray triangles are double layer domains. These show that most of the MoS_2 film was a single crystal of monolayer thickness.

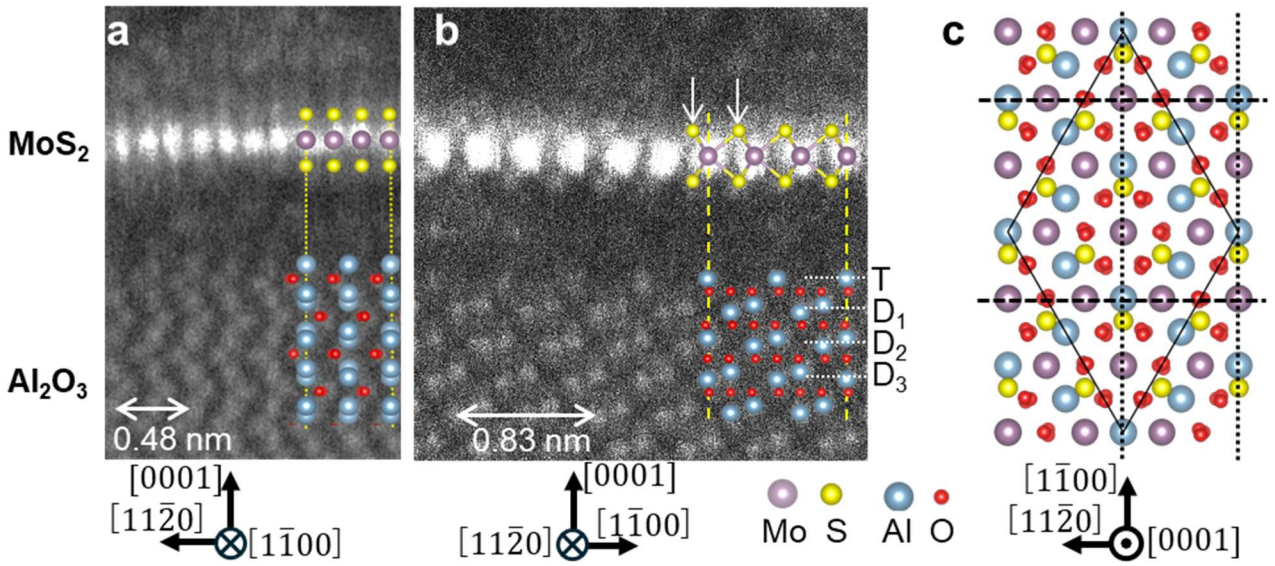

Fig. 2 (a) (b) HAADF-STEM image of monolayer-MoS_2/α-Al_2O_3 viewed in [1$\bar{1}$00] and [11$\bar{2}$0] direction of α-Al_2O_3. Atomic models of pristine MoS_2 and Al_2O_3 are overlaid. In (b), T indicates the Al_2O_3 surface, which is terminated with a single Al atomic layer (the Al-I structure), whereas D_1 and D_2 indicate pairs of closely spaced Al atomic layers. The positions of Mo atoms coincide with those of the Al (11$\bar{2}$0) planes on the dotted line in (a). The atomic positions of Mo coincide with those of surface Al-I atoms on the vertical dashed lines in (b). In (b), downward arrows show that the lateral distance between a Mo and neighboring S atoms is smaller on the left-hand side of the Mo atom than on the right-hand side. (c) Atomic model of monolayer-MoS_2 on α-Al_2O_3 structure based on the HAADF-STEM image in (a) and (b). The dotted and dashed lines indicate the Al atomic plane of α-Al_2O_3 and correspond to the dotted lines in (a) and dashed line in (b).

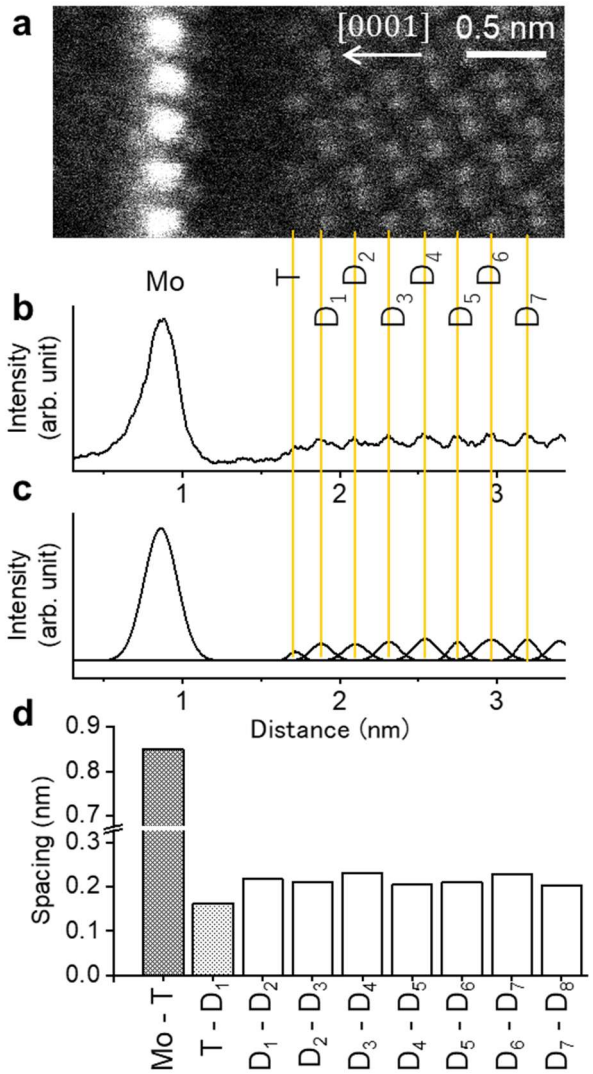

Fig. 3 (0001) layer spacing in MoS_2/α-Al_2O_3 structure. (a) $[11\bar{2}0]$ HAADF-STEM image. (b) Image intensity distribution in the [0001] direction in (a). The peak denoted as T is the intensity peak due to surface Al-I atoms. Peaks D_n are due to pairs of closely spaced Al-I and II layers. (c) Gaussian curves fitted to peaks in (b). The centers of the Gaussian curves are used as the positions of peaks. (d) Lattice spacings in (c).

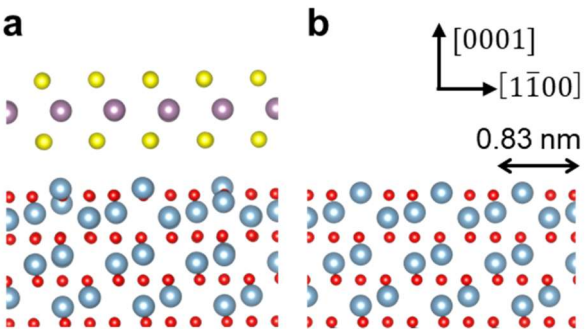

Fig. 4 Theoretical atomic models of (a) fully relaxed MoS_2/α-Al_2O_3 structure (model A) and (b) α-Al_2O_3 surface without MoS_2 (model B). No interface layer was assumed in these calculations. Atoms are marked using the same colors as in Fig. 2.